Flora 241 (2018) 27–34

Contents lists available at ScienceDirect

Flora

journal homepage: www.elsevier.com/locate/flora

Leaf margin organisation and the existence of vaterite-producing hydathodes in the alpine plant *Saxifraga scardica*

Raymond Wightman[a,*], Simon Wallis[b], Paul Aston[b]

[a] Microscopy Core Facility, Sainsbury Laboratory, University of Cambridge, Bateman Street, Cambridge, CB2 1LR, UK
[b] Cambridge University Botanic Garden, 1 Brookside, Cambridge CB2 1JE, UK

ARTICLE INFO

Edited by Alessio Papini

Keywords:
Calcite
cryoSEM
Hydathode
Leaf margin
Saxifraga
Vaterite

ABSTRACT

Some sections of species within the genus *Saxifraga* deposit a chalky crust on the surface of their leaves, originating from the guttation medium produced by the sunken hydathodes found generally at or near the leaf margin. The organisation of the hydathode tissues, that of the rest of the leaf and the physiology of the crust is poorly understood. We have used cryo-SEM and cryo-fracture to study leaf tissue organisation and structure in *Saxifraga scardica* and compared it to the imaging data with the previously characterised *Saxifraga cochlearis*. We find *S. scardica* contains a transparent and tapered leaf margin containing thick walled cylindrical cells that may serve to deflect light to the adjacent palisade mesophyll tissue. Raman microscopy reveals the *S. scardica* leaf crust contains the rare and metastable calcium carbonate polymorph vaterite whereas the crust from *S. cochlearis* contains only calcite. Vaterite-crust is also observed on the leaves of some species within the section *Porphyrion* but is not found on members of the section *Ligulatae*. The implications of these findings are discussed.

1. Introduction

The genus *Saxifraga* comprises approximately 400 species, arranged within sections and subsections based on molecular and morphological characteristics (Gornall, 1987a). Those species comprising encrusted leaves as a result of guttation from hydathode structures termed “chalk glands” are found in sections *Ligulatae, Xanthizoon* and *Porphyrion* (for detailed discussion and molecular taxonomic analysis of the *Saxifraga* see Conti et al., 1999 and Tkach et al., 2015). The leaves of these and other sections are commonly small and fleshy. Information on *Saxifraga* leaf anatomy is often patchy. Detailed drawings of arctic *Saxifraga* have given an insight in to epidermal and, to some extent, mesophyll organisation (Galløe, 2010). *Saxifraga* leaves appear to have dorsiventral mesophyll organisation and a thick leaf cuticle as demonstrated for *Saxifraga hirculus* and *Saxifraga paniculata* (Codignola et al., 1990; Pyankov et al., 1999). Alpine *Saxifraga* species generally have a defined visible boundary between palisade and spongy mesophyll whereas for arctic species the distinction is less clear (Galløe, 2010). For alpine desert plants, the dorsiventral organisation of mesophyll is speculated to aid photosynthesis at high irradiation but at a cost to decreased drought tolerance (Pyankov et al., 1999). It is known that hydathodes consist of thin walled epithem tissue and, where they are found to be sunken within the leaf, extrude guttation medium to fill the pit and adjacent leaf margin area as observed for *Saxifraga cochlearis* and *Saxifraga crustata* (Gardiner, 1881; Wightman et al., 2017). In *S. paniculata* (synonym *S. aizoon*), the plastids of epithem cells have been shown to contain electron dense structures of phytoferritin and may be the principal site of synthesis or storage within the plant (Perrin, 1970). Encrusted species, as a rule, tend to possess these pits, often termed “cavities” whereas non-encrusted *Saxifraga* species have hydathodes positioned close to the leaf surface (Galløe, 2010). Some non-encrusted species instead contain internal calcium oxalate structures termed foliar crystals that may have an analogous role to the crusted hydathodes (Gornall, 1987b). For *S. cochlearis* the crust consists of the calcium carbonate polymorph calcite (Wightman et al., 2017). Leaf trichomes, where observed, tend to possess multiseriate morphology for the encrusted species (Gornall, 1986). A thorough comparative analysis of leaf venation patterns show camptodromous veins within the encrusted species where the open vein system has been proposed to be well adapted to extruding the calcium salts (Zhang et al., 2015).

Saxifraga scardica is a member of the section *Porphyrion*. Its name originates from where it was discovered, in 1839, by Grisebach on the two main peaks of the Sar Planina in the Scardus mountain range of the Balkans. Its distribution sees it extend though northern Montenegro, Kosovo, Albania and in to Greece. It commonly grows at altitudes between 1800 and 2500 m on limestone rocks in both alpine and subalpine zones. It reaches altitudes as high as 2900 m on sunny positions of Mount Olympus to as low as 400 m in nearby ravines and the Treska

* Corresponding author.
E-mail address: raymond.wightman@slcu.cam.ac.uk (R. Wightman).

https://doi.org/10.1016/j.flora.2018.02.006
Received 19 September 2017; Received in revised form 9 February 2018; Accepted 12 February 2018
Available online 14 February 2018

gorge (Strid and Tan, 1986; Webb and Gornall, 1989). *Saxifraga scardica* forms a compact and dense cushion that over time can form hummocks or low mats. The stiff and spiny rosettes are 10–15 mm in diameter and leaves are 5–15 mm x 2–4 mm lanceolate to spathulate with a tip described as acute/mucronate. The leaves are fleshy and vary in colour from dark to light green and the surface of the leaf is convex with the tip being distinctly keeled inwards. It has been documented that the *S. scardica* leaves have "translucent margins" (Webb and Gornall, 1989) and further described as having "cartilaginous edges" (Irving and Malby, 1914; Smith and Fitch, 1909). Hydathodes occur at the edge of the leaf and number between 9 and 15. The inflorescence consists of cup shaped flowers which flatten as they open. The petals are commonly conspicuous 7–12 mm obovate, overlapping to slightly separate and are white sometimes fading to pink, however, the shape and colour of these petals as well as other attributes can vary (Horný et al., 1986).

Given that *S. scardica* is found in a distinct section compared to the recently characterised *S. cochlearis* and appears to have key differences in leaf morphology, we examined the ultrastructure, composition and physiology of *S. scardica* leaves with a focus on the hydathodes and transparent margin. We report notable differences between the two species that include the crystal structure of the crust and the precise arrangement of the mesophyll. We extend the molecular analysis of the crust to other *Saxifraga* species. We demonstrate the *S. scardica* margin is a unique tissue with light deflection properties that may serve to aid light capture by the leaves.

2. Materials and methods

2.1. Propagation and growth of studied Saxifraga species

The *Saxifraga* used in this study were (i) section *Porphyrion* species *S. scardica* Griseb., *S. diapensioides* Bellardi, *S. sempervivum* K. Koch, *S. ferdinandi-coburgi* Kellerer & Sünd. and (ii) section *Ligulatae* species *S. cochlearis* Rchb., *S. longifolia* Lapeyr., *S. valdensis* DC., *S. paniculata* Mill., *S. callosa* Sm. var. *australis* (Moric.) D.A. Webb and *S. crustata* Vest. All plant samples were grown at the Cambridge University Botanic Garden (52.1935°N, 0.1258°E), in terracotta pots containing a loam based peat free John Innes compost with extra grit. The pots have been plunged in sand beds to maintain correct moisture levels. For propagation, single rosette cuttings from post-flowering plants were grown in a mix of equal parts sharp sand, grit and perlite. Plants were grown under an open sided polytunnel and watered by hand using collected rain water. Care was taken to avoid excessive exposure to the sun as recommended by Harding (Harding, 1981). Leaves were harvested and observed in June for cryoSEM and light microscopy. For Raman analysis of the crust, leaves were harvested according to the schedule in the legend of Table 1. Leaves for all analyses were taken from non-flowering stems at a developed stage intermediate in size between the youngest leaves visible at the apex and the first fully grown leaves in the upper half of the rosette.

Table 1
Survey of crust polymorph composition in *Saxifraga* species revealed by Raman microscopy. Samples were taken and assayed at three time points: April/May 2016 (Assay 1), March 2017 (Assay 2) and May 2017 (Assay 3, for confirming vaterite-containing leaves).

Saxifraga species	Assay 1	Assay 2	Assay 3
S. cochlearis	C	C	C
S. scardica	VC	VC	VC
S. longifolia	C	C	nd
S. valdensis	C	C	nd
S. paniculata	C	C	nd
S. diapensioides	V	V	VC
S. sempervivum	V	V	V
S. ferdinandi-coburgi	V	VC	VC
S. callosa	C	C	nd
S. crustata	C	C	nd

C = Calcite, V = Vaterite, VC = Vaterite/Calcite mixture, nd = assay not done.

2.2. Stereo, light and confocal microscopy

Stereomicroscopy (Fig. 1A, B) was carried out using a Zeiss V20 stereomicroscope fitted with a 1x PlanApo S objective and a Zeiss AxioCam HRc camera. Uniform illumination of samples was achieved using a Schott ring light from above and a gooseneck light pair from the sides. Axiovision software (Zeiss) was used for acquisitions that comprised a Z-stack that encompassed the entire focal depth of the sample followed by the Extended Depth of Field plugin for producing a single in-focus image from the z-stack. Transmitted light microscopy of leaf margins (Fig. 3A, B) used a Leica DM1000 microscope, 20x objective and a Leica ICC50 W camera. Confocal microscopy (Fig. S4) for imaging ultra-violet (UV) autofluorescence was carried out on hand-cut transverse sections of leaves mounted in water with a coverslip and viewed using an upright Leica SP8 confocal microscope fitted with a 20x dry objective lens. The 405 nm laser was set to 28% and the detection range was set to 420–551 nm (blue/green) and 646–697 nm (red). The transmitted light channel used the 561 nm laser set to 9%. Two leaves were sectioned and imaged, one is shown in Fig. S4 and the other gave the same result.

2.3. Cryo-scanning electron micoscopy (cryoSEM)

Leaves (3x *S. cochlearis* and 3x *S. scardia*) were arranged and observed in paired sets, one from each species, on cryo-stubs ready for cryoSEM preparation. CryoSEM was carried out according to the protocol described in Wightman et al. (Wightman et al., 2017) with the following modifications: (i) The time between harvesting the *S. scardica* leaf and plunge freezing in the liquid nitrogen was less than 5 min to avoid the undesirable drying of leaf internal tissues. (ii) The Zeiss EVO HD15 SEM used either the secondary electron (SE) detector, with 4–5 nm of platinum coating to enhance contrast, or the backscattered electron detector (BSD, with 1.5–3 nm coating to eliminate sample charging. (iii) The accelerating voltage was set to 8 kV (SE imaging) or 25 kV (BSD imaging). The I probe was set to 2.4 nA for both forms of imaging.

2.4. Raman microscopy

Raman point spectra and map data were produced from encrusted leaves found close to the vegetative stem apex, using a Renishaw InVia Raman microscope fitted with a 50 x dry objective and a 532 nm laser. Leaves were placed on a stainless steel slide with no coverslip. Point spectra (Fig. 2A and Table 1) were generated after 1 s exposure time, 3x accumulation, laser power of 50% and a spectral centre set to 750 cm^{-1} and pinhole engaged. Raman mapping used the StreamlineHR function of the InVia with the 532 nm laser set to 5%, 0.8 s exposure, no accumulation, pinhole disengaged and a spectral centre set to 750 cm^{-1}. Raman analysis of the transparent leaf margin had the 532 nm laser set to 50% power, 4 s exposure, 3x accumulation and spectral centre set to 1250 cm^{-1}. Raman peaks were assigned by comparing to the reference assignments reported by Schulz and Baranska (2007).

2.5. Comparisons of cryoSEM and Raman data with Arabidopsis interfascicular fibres

The same cryoSEM and Raman apparatus used for *Saxifraga* research is used extensively for analysis of cell wall ultrastructure and chemistry in the secondary wall forming tissues of the xylem and fibres in the model plant *Arabidopsis thaliana* Heynh. (R. Wightman, unpublished data) and this work provided the link in terms of the striking morphological similarities between *S. scardica* margin cells and *Arabidopsis* fibres. Stems from *Arabidopsis* ecotype Landsberg *erecta*

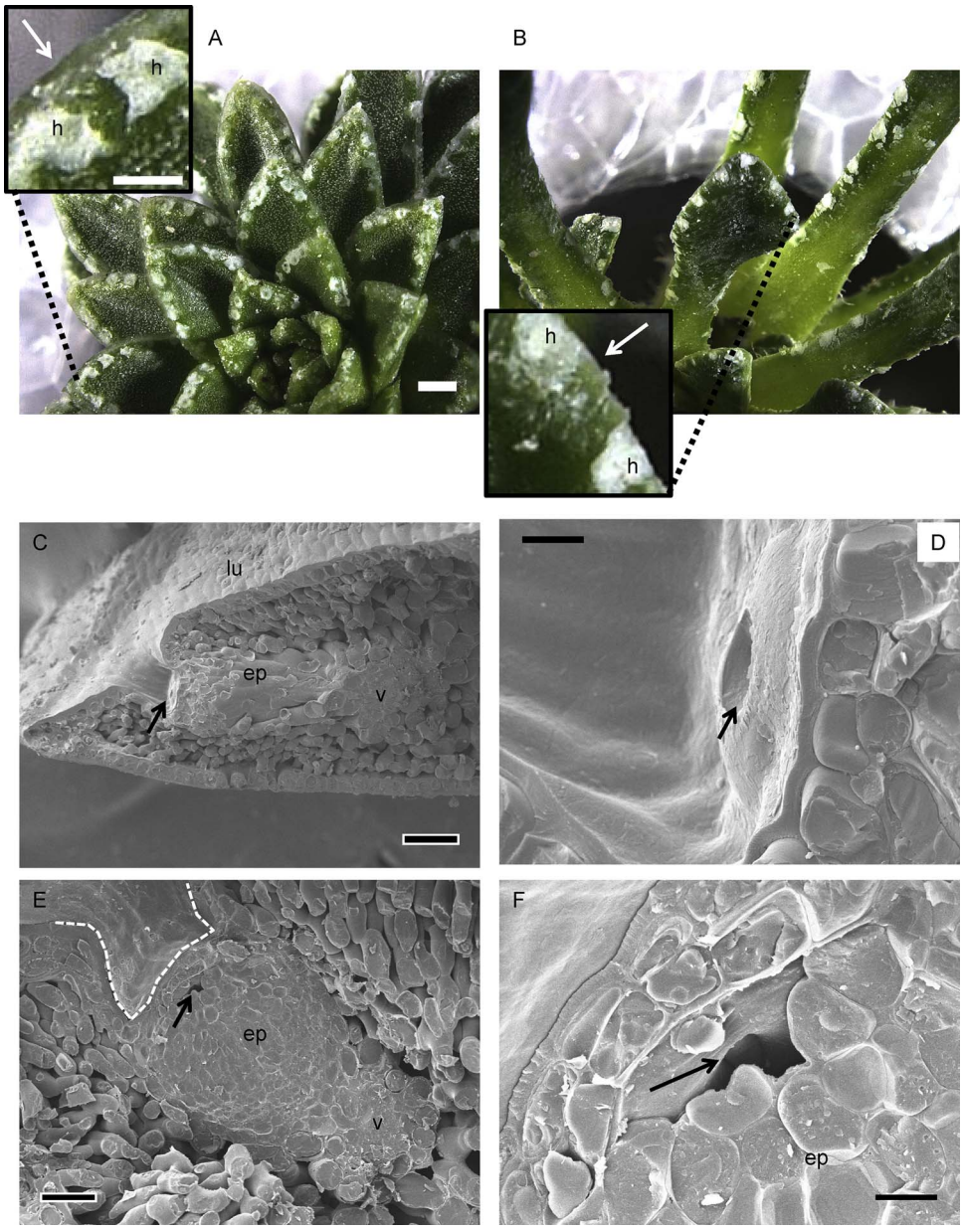

Fig. 1. Leaf hydathode structure of S. scardica. (A) Extended depth of field stereomicroscopy of *S. scardica* leaves with magnified view (inset) showing encrusted hydathodes (h), and compared to *S. cochlearis* (B). The location of the leaf edge is marked by a white arrow. Scale bar in A = 1 mm, B = 0.5 mm. (C-F) SEM images taken of cryo-fractured *S. scardica* leaves. (C) Hydathode pit region and magnified area of the pit base (D) showing the rim of the hydathode pore (arrows). (E) Fracture through the epithem tissue showing small packed cells and an airspace (arrow) below the pit base. The outline of the pit is shown as a white dashed line. (F) Magnified view of the airspace (arrow) and epithem cells. Scale bars C = 100 µm, D = 10 µm, E = 100 µm, F = 10 µm. Abbreviations: lu, leaf upper surface; ep, epithem tissue; v, vasculature.

were collected from fully grown plants grown in 16hr light regimes in a controlled environmental growth chamber. For cryoSEM stems were placed upright in a cryoEM stub before cryo-processing and fracture and then imaged as for *Saxifraga*. For Raman, thin hand-cut transverse sections were placed on a slide containing water and a coverslip added to prevent movement during Raman acquisitions. Raman acquisition settings were the same as for the *S. scardica* leaf margin settings described above.

2.6. Light deflection assay

The light deflection assay (Movies S1-S3) used a Zeiss Axioimager.M2 microscope fitted with a HXP 120C fluorescence light source, a Hamamatsu ImagEM–1K camera and a 20x dry objective. The incident light, shone onto the sample, was from the violet/indigo part of the spectrum, generated using a 438/24 nm excitation filter in combination with a 458 nm edge dichroic beamsplitter (Laser2000 (UK) Ltd, Huntingdon, UK). Autofluorescence was detected in the green/yellow part of the visible spectrum using a 542/27 nm emission filter (Laser2000 (UK) Ltd). To create a narrow beam, the field diaphragm was set to minimum. The beam was slowly moved, via the microscope stage controls, across the leaf margin and recorded live using the Fast Acquisition plugin of the Zeiss Axiovision software. The beam itself is visible when on the leaf margin due to tissue autofluorescence at that site. Any deflection of incident light from the beam spot on leaf margin would result in additional autofluorescence coming from the adjacent green tissue.

3. Results

3.1. Saxifraga scardica hydathode, pit and leaf epidermal structure

A top view of the *S. scardica* leaf (Fig. 1A) shows encrusted hydathode pits arranged at regular intervals along the leaf edges with a similar arrangement to *S. cochlearis* (Fig. 1B). One notable difference is the proximity of hydathodes to the margin, located closer to the margin in *S. cochlearis* than in *S. scardica*. Random transverse cryofractures were generated and the frozen tissue was observed using SEM. Cryopreservation was notably more difficult for *S. scardica* than for *S. cochlearis*, initially resulting in extensive drying of internal tissues

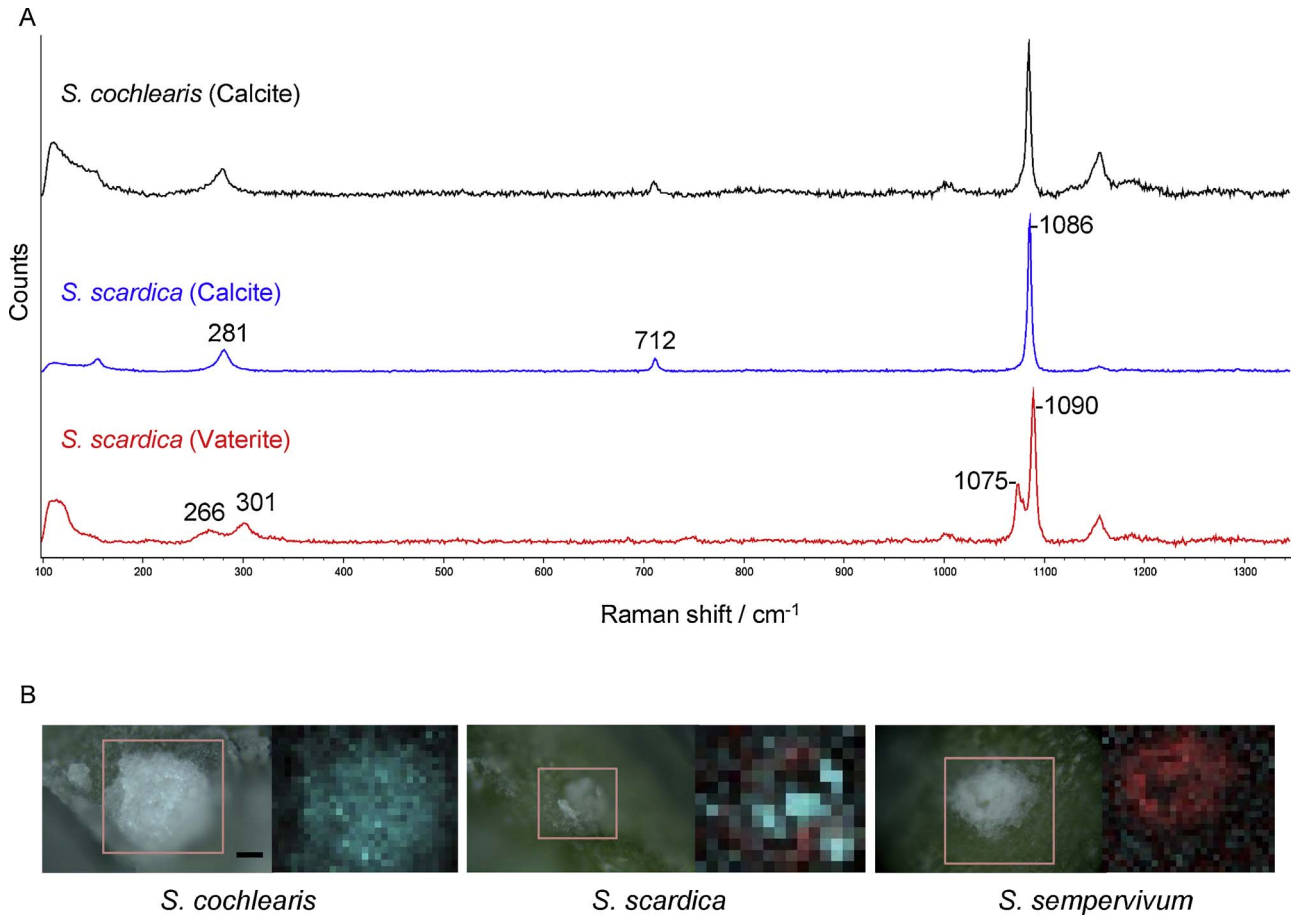

Fig. 2. Raman microscopy of surface crust. (A) Raman spectra from hydathode deposits of *S. cochlearis*, showing the characteristic 1086 cm^{-1} calcite peak, together with two types of spectra obtained for *S. scardica*. Shown are average spectra from three locations of a hydathode pit. In *S. scardica* assays were taken from hydathodes filled with only calcite or only vaterite. (B) Raman imaging showing intensity maps of calcite (plotted 1086 cm^{-1}, cyan) and vaterite (plotted 1090 cm^{-1}, red) in hydathode pits for *S. cochlearis*, *S. scardica* and *S. sempervivum*. Scale bar = 50 µm.

resulting in shriveled cells and ruptured tissues. This was remedied by reducing the time interval between leaf harvesting and plunge freezing to less than 5 min, suggesting the extensive drying occurred after the leaf is detached from the stem. Some fractures occurred within or in the vicinity of hydathodes showing steep-sided pits and underlying epithem tissue that appeared continuous with the vasculature (Fig. 1C). The hydathode pit base has a rim surrounding a pore (Fig. 1D) and a closer view of a fracture through the epithem tissue reveals tightly packed cells (Fig. 1E) with a space below the centre of the pit base, presumably in the vicinity of the pore (Fig. 1E, F). No intercellular spaces are seen between epithem cells (Fig. 1E, F). The epidermal layer of the *S. scardica* leaf have very thick wall/cuticle regions, similar to *S. cochlearis* (Fig. S1) with the wall/cuticle being densely packed and of a thickness that is in excess of 15 µm.

3.2. Constituents of the leaf crust in S. scardica and related species

We used Raman microscopy to determine the composition of the crusty deposits of material that arise as a result of hydathode guttation. Fig. 2A shows the Raman spectra of crust from *S. scardica* and are compared to that of the calcite spectrum previously demonstrated for *S. cochlearis* (Wightman et al., 2017). Two distinct types of spectra are produced for *S. scardica*: Firstly, a prominent peak at 1086 cm^{-1} and two minor peaks at 712 cm^{-1} and 281 cm^{-1} are similar to those from *S. cochlearis* and match those expected for calcite (Jorge Villar and Edwards, 2006). The second spectrum sees the prominent peak shift to 1090 cm^{-1} and a second peak emerge at 1075 cm^{-1} (Fig. 2A). These peaks are both within the region of the spectrum characteristic of carbonates, however, a match was not found within Raman databases for minerals (http://www.geologie-lyon.fr/Raman/). This Raman peak-doublet of 1075–1090 cm^{-1}, together with the peaks at 266 cm^{-1} and 301 cm^{-1}, match those identified from the small amounts of biomineralised vaterite taken from the Antarctic clam and Coho Salmon (Gauldie et al., 1997; Nehrke et al., 2012). This means vaterite coexists with calcite on the surface of the *S. scardica* leaf. To confirm this, Raman mapping was carried out on an encrusted hydathode pit region where calcite is plotted as intensity at 1086 cm^{-1} and vaterite at 1090 cm^{-1}. *Saxifraga cochlearis* crust consists only of calcite (Fig. 2B) whereas an encrusted hydathode pit region was mapped showing both calcite and vaterite for *S. scardica*. We found another species, *Saxifraga sempervivum*, only gave vaterite spectra (Fig. 2B, Table 1). We then surveyed several species across the genus and discovered a further two vaterite producers: *S. diapensioides* and *S. ferdinandi-coburgi*. In addition to *S. cochlearis*, we detected calcite without any vaterite in *S. longifolia*, *S. valdensis*, *S. paniculata*, *S. callosa* and *S. crustata* (Table 1).

3.3. Leaf margin structure and function in S. scardica

In contrast to *S. cochlearis*, *S. scardica* possesses a thick, partially transparent leaf margin (Fig. 3A, B). SEM after cryofracture reveals *S. cochlearis* to have steep-sided margins compared to the pointed and tapered *S. scardica* margin. The palisade tissue layer, consisting of tightly packed cells, extends to the margins in *S. cochlearis* but the palisade layer extends round the inside of the tapered margin in *S. scardica* (Fig. 3C). Magnified views find that the small margin point in *S. cochlearis* is formed from the epidermal cell layer (Fig. 3D) whereas the

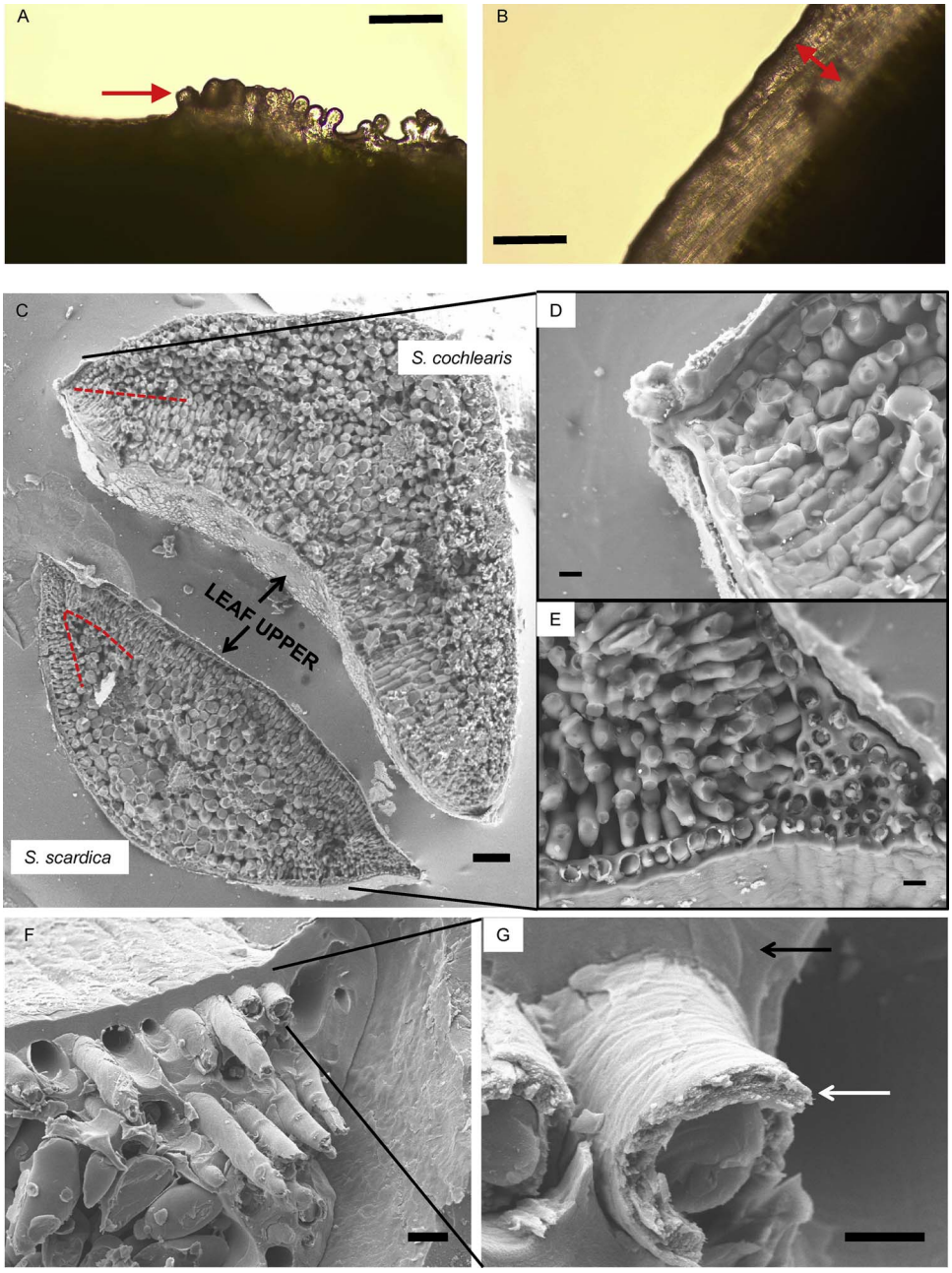

Fig. 3. Leaf margin ultrastructure. (A, B) Light microscopy images showing the leaf margin of *S. cochlearis* (A) compared to *S. scardica* (B). Red arrows point to the transparent part of the leaves; to lobe teeth in (A) and a thick margin rim in (B). Scale bars = 100 µm. (C-E) Backscattered electron SEM imaging directly comparing transverse cryofractures of leaves from *S. cochlearis* and *S. scardica*. The margin of *S. scardica* (E) is tapered and extended compared to that of *S. cochlearis* (D). Red dashed lines in (C) show approximate boundary between palisade and mesophyll layers. Note that in *S. scardica*, the palisade layer appears to extend to below the leaf margin. (F, G) SEM secondary electron imaging of a *S. scardica* oblique cryofracture showing the cylindrical cells that make up the transparent leaf margin region. A magnified view in (G) shows secondary walls (white arrow) that are distinct from the walls that surround the leaf epidermis (black arrow). Scale bars C = 200 µm, D,E,F = 20 µm, G = 5 µm. (For interpretation of the references to colour in this figure legend, the reader is referred to the web version of this article.)

tapered *S. scardica* margin is formed from an ordered array of thick walled cylindrical cells (Fig. 3E, F). These long, narrow cells appear to possess a secondary wall (Fig. 3G) with an ultrastructure resembling the cellulose-rich cells of stem interfascicular (sclerenchyma) fibres from the model plant, *Arabidopsis thaliana*. (Fig. S2). Raman microscopy of the leaf margin interior reveals an abundance of pectin (856 cm^{-1}) and cellulose (1091/1120 cm^{-1}) with strong carotenoid signal represented by 1001, 1155 and 1522 cm^{-1} peaks (Fig. 4A: Schulz and Baranska, 2007). This is a different composition to the interfascicular fibre tissues which have cellulose impregnated with lignin, represented by prominent peaks at 1596 and 1656 cm^{-1} (Fig. S3). Pectin (856 cm^{-1}), although will be present in the middle lamella, is not in sufficient quantities in the stem fibre tissue to be detected by Raman. Autofluorescence of the *S. scardica* leaf margin, detected by a confocal microscope after 405 nm excitation, gives high signal for the leaf cuticle, lignified xylem and chloroplasts but very low signal for cells within the transparent margin suggesting fluorescent species such as lignin are absent or in very low quantities (Fig. S4).

Given that (i) the tapered margin is transparent (ii) the thick walls have the morphology of a secondary wall forming tissue but an atypical composition (iii) the palisade layer extends round the leaf margin, we explored the possibility that the margin might be structured to deflect light in to the leaf (Fig. 4B). To do this, an upright fluorescence microscope was used to give a narrow beam or “spot” of blue light. The leaf margin was then slowly moved under the spot. Any directional deflection of the beam in to the leaf would be seen as chlorophyll autofluorescence from the green tissue (Fig. 4C). For *S. cochlearis*, when the narrow beam reaches the leaf margin, a faint light diffraction signal is observed in all directions (Movie S1). This experiment was repeated a further 3 times and yielded the same result. For *S. scardica*, four experiments (two are shown in movies S2 and S3) all resulted in a deflection of the incident light from the transparent margin to the direction of the leaf green tissue resulting in chlorophyll autofluorescence.

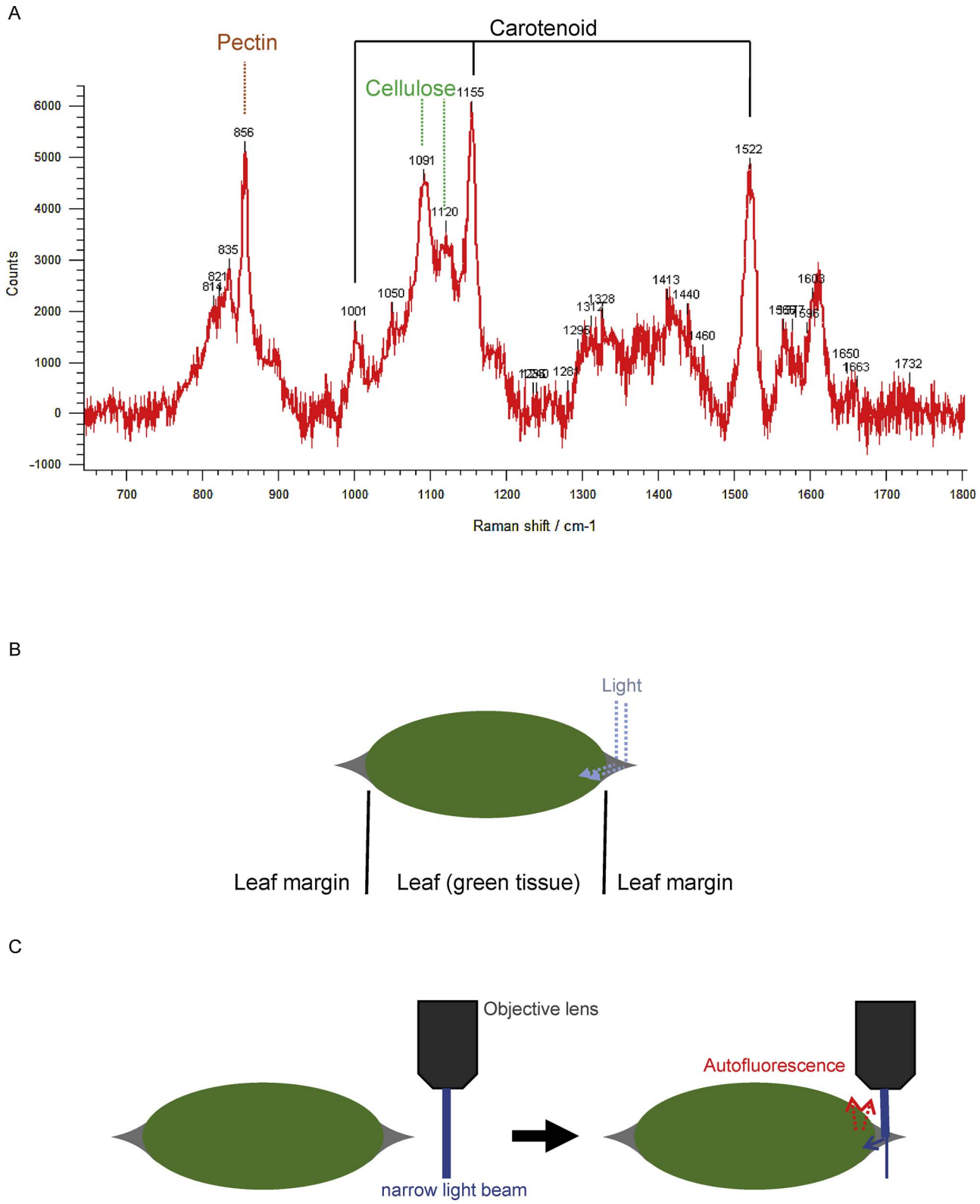

Fig. 4. Leaf margin composition and light deflection experimental design. (A) Raman spectrum measured from the interior (approximately 40 μm deep) of the *S. scardica* transparent leaf margin. Peaks assigned to pectin, cellulose and carotenoid are labelled. (B) The leaf schematic shows the path of light in to the green tissue if it were to be deflected by the walls of the margin. (C) Illustration showing the design of the light-deflection experiment. A narrow beam of light is created out of the centre of the objective lens and the margin region is moved to beneath the beam. Any deflection (blue arrow) will be detected by auto-fluorescence emanating from the adjacent green tissue (red arrows).

4. Discussion

The *S. scardica* leaf hydathode has similarities to that previously characterised for *S. cochlearis* (Wightman et al., 2017); steep-sided pits, a thick rimmed hydathode pore and epithem tissue consisting of tightly packed regular-shaped cells. The epithem of *S. cochlearis* was shown to lack the intercellular spaces that are commonly found in hydathodes from a diverse range of plants (Wightman et al., 2017). This may be

common to all encrusted saxifrages given *S. scardica* also lacks such spaces, as does *S. paniculata* (Andrei and Paraschivoiu, 2008). Guttation fluid may be held in the void found at the interface between epithem and the pit base. Despite the similarities in hydathode morphology, *S. scardica* produces vaterite which has not been demonstrated for *S. cochlearis*. The vaterite structure is characterised as a metastable calcium carbonate polymorph representing a short-lived, or transient, phase between the amorphous and calcite phases (Christy, 2017). Fewer properties are known for vaterite, compared to the abundant and stable calcite polymorph (Chakoumakos et al., 2016). Vaterite dissolves more readily in the human body making it a highly desirable constituent of drug delivery vehicles (Parakhonskiy et al., 2012). Recent data suggest that the vaterite crystal is a mosaic of two structures (Kabalah-Amitai et al., 2013). It is generally not found in nature, apart from meteorites and some biomineralised structures from aquatic organisms (Lowenstam and Abbott, 1975; Gauldie et al., 1997; Newton, 2007; Nehrke et al., 2012). This instability makes it difficult to produce vaterite in industrial or pure quantities, however, to have some vaterite existing on the surface of a leaf in an outdoor cultivated environment is a significant finding. We examined other *Saxifraga* species grown at the same site and sampled in the year 2016 and then in 2017. Like *S. scardica*, *S. diapensioides* and *S. ferdinandi-corburgii* had evidence of vaterite as well as calcite in the leaf crust. Raman analysis of the crust of *S. sempervivum* only showed the presence of vaterite (Fig. 2). All these species have in common a taxonomic relationship, they have been classified as members of the section *Porphyrion* whereas the non-vaterite producers are classified within the section *Ligulatae* (Gornall et al., 2015). A detailed molecular phylogeny of *Saxifraga*, yielding a revised and improved classification of the genus, confirms the assignment of these species to one of these evolutionary distinct groups (Tkach et al., 2015). Using this classification we can begin to survey other related species to determine the extent of vaterite production within the genus. Ebersbach et al. (2017) detected a rate-shift of diversification within section *Porphyrion* that was attributed, in part, to the development of encrustated hydathodes and may account for the acquisition of vaterite deposition. One proviso concerning our data is that it represents cultivated material from a temperate oceanic climate, specifically Cambridge UK, and it is yet to be determined if vaterite exists in their native locations at generally much higher altitudes. The finding does not answer the questions as to why encrustation by vaterite exists and how this is achieved. Vaterite may have optical or thermal properties that have been exploited by the *Porphyrion* species. The seeding and stability of the polymorph on the leaf exterior may be attributed to a trace substance, such as a metal, or a vaterite-inducing peptide similar to the pelovaterin that has been isolated and characterised from the turtle *Pelodiscus sinensis* Wiegmann (Lakshminarayanan et al., 2005).

Saxifraga scardica possesses a largely transparent leaf margin region, devoid of green tissue that is not found in *S. cochlearis*. Cryofractured transverse sections of *S. scardica* leaves show this transparent region to be tapered. In both *S. scardica* and *S. cochlearis*, a thick outer cell wall exists in the epidermal cell layer of the leaves. These thick-walled cells make up the margin region of *S. scardica* (Fig. 3) together with long cylindrical cells that bear morphological similarities to interfasicular fibres. These fibre-type cells are the likely source of the historical description of *S. scardica* leaf edges being cartilaginous (Irving and Malby, 1914). Raman microscopy show the walls are a pectin-rich cellulosic matrix and not the typical lignocellulose seen in woody secondary wall tissues such as fibres. Although woody tissues will have some pectin, found mostly within the middle lamellae, this is not detectable in our Raman protocol which only detects the most abundant molecular species. The transparent margin tissue deflects a beam of light. Although we cannot account for differences in leaf curvature between *S. cochlearis* and *S. scardica*, the data suggest one role of the margin in the latter is for light deflection to the marginal palisade cells. It is not known if this property is an adaptive function of the *S. scardica* margin, however, we see in cryofractures the palisade layer to come around the edge of the margin. It is hard to identify why the palisade cells would be positioned here if not for harvesting light energy and may be an adaptation to deal with sometimes living in low-light or shaded areas such as deep gorges or north facing aspects (Strid and Tan, 1986). A leaf inherently has the properties to focus light and change its direction, influenced by cell shape, tissue organisation and cell wall arrangements (Vogelman et al., 1996a; Vogelmann et al., 1996b; Lee, 2009; Brodersen and Vogelmann, 2010). Some specialised light channeling or light focusing structures are found across the plant kingdom, a prime example being the leaf windows of succulent plants such as those at the leaf tips of Mesembryanthemaceae (Krulik, 1980). The *S. scardica* leaf margin is potentially another example of such an optical device.

5. Conclusion

Saxifraga scardica leaves contain potentially useful materials and biocomposites for exploitation, including the rare mineral polymorph vaterite and bioinspired optics.

Acknowledgement

The Microscopy Facility at the Sainsbury Laboratory is supported by the Gatsby Charitable Foundation. We are grateful for the opportunity to access the Saxifrage collection at Cambridge University Botanic Garden.

Appendix A. Supplementary data

Supplementary data associated with this article can be found, in the online version, at https://doi.org/10.1016/j.flora.2018.02.006.

References

Andrei, M., Paraschivoiu, R.M., 2008. Anatomical researches on the overground vegetative organs of *Saxifraga mutata* L. subsp. *demissa* (Schott & kotschy) D.A. webb and *Saxifraga paniculata* miller. An. Stiint. Univ. Al. I. Cuza Iasi, Sect. II a. Biol. Veget. 54 (2), 5–14.
Brodersen, C.R., Vogelmann, T.C., 2010. Do changes in light direction affect absorption profiles in leaves? Funct. Plant Biol. 37, 403.
Chakoumakos, B.C., Pracheil, B.M., Koenigs, R.P., Bruch, R.M., Feygenson, M., 2016. Empirically testing vaterite structural models using neutron diffraction and thermal analysis. Sci. Rep. 6, 36799.
Christy, A.G., 2017. A review of the structures of vaterite The impossible, the possible, and the likely. Cryst. Growth Des. 17, 3567–3578.
Codignola, A., Fieschi, M., Maffei, M., Fusconi, A., 1990. Leaf anatomy and photosynthetic characteristics of succulent alpine plants growing at high elevations. Nord. J. Bot. 10, 49–56.
Conti, E., Soltis, D.E., Hardig, T.M., Schneider, J., 1999. Phylogenetic relationships of the rilver saxifrages (*Saxifraga*, sect. *Ligulatae* Haworth) Implications for the evolution of substrate specificity, life histories, and biogeography. Mol. Phylogenet. Evol. 13, 536–555.
Ebersbach, J., Schnitzler, J., Favre, A., Muellner-Riehl, A.N., 2017. Evolutionary radiations of the species-rich mountain genus *Saxifraga* L. BMC Evol. Biol. 17, 119.
Galløe, O., 2010. The biolocical leaf-anatomy of the Arctic species of *Saxifraga*. Medd. om Grønl. 36, 237–294.
Gardiner, W., 1881. Memoirs: the development of the water-glands in the leaf of *Saxifraga crustata*. J. Cell Sci. s2–21.
Gauldie, R.W., Sharma, S.K., Volk, E., 1997. Micro-raman spectral study of vaterite and aragonite otoliths of the coho salmon, *Oncorhynchus kisutch*. Comp. Biochem. Physiol. Part A Physiol. 118, 753–757.
Gornall, R.J., Zhang, Z., Chen, S., 2015. Morphology and anatomy of the exine in *Saxifraga* (Saxifragaceae). Phytotaxa 212, 105.
Gornall, R.J., 1986. Trichome anatomy and taxonomy of *Saxifraga* (Saxifragaceae). Nord. J. Bot. 6, 257–275.
Gornall, R.J., 1987a. An outline of a revised classification of *Saxifraga* L. Bot. J. Linn. Soc. 95, 273–292.
Gornall, R.J., 1987b. Foliar crystals in *Saxifraga* and segregate genera (Saxifragaceae). Nor. J. Bot. 7 (3), 233–238.
Harding, W., 1981. Saxifrages. The Alpine Garden Society, London.
Horný, R., Webr, K.M., Byam-Grounds, J., 1986. Porophyllum Saxifrages. The Byam-Grounds Publications.
Irving, W., Malby, R., 1914. Saxifrages or Rockfoils. Swarthmore Press Ltd., London.
Jorge Villar, S.E., Edwards, H.G.M., 2006. Raman spectroscopy in astrobiology. Anal. Bioanal. Chem. 384, 100–113.

Kabalah-Amitai, L., Mayzel, B., Kauffmann, Y., Fitch, A.N., Bloch, L., Gilbert, P.U.P.A., Pokroy, B., 2013. Vaterite crystals contain two interspersed crystal structures. Science 340, 454–457.
Krulik, G.A., 1980. Light transmission in window-leaved plants. Can. J. Bot. 58, 1591–1600.
Lakshminarayanan, R., Ooi Chi-Jin, E., Jun Loh, X., Kini, R.M., Valiyaveettil, S., 2005. Purification and characterization of a vaterite-inducing peptide, pelovaterin, from the eggshells of *Pelodiscus sinensis* (Chinese soft-shelled turtle). Biomacromolecules 6, 1429–1437.
Lee, D.W., 2009. Plant tissue optics: micro- and nanostructures. Proc. SPIE Conf. 7401.
Lowenstam, H., Abbott, D., 1975. Vaterite: a mineralization product of the hard tissues of a marine organism (Ascidiacea). Science 188, 363–365.
Nehrke, G., Poigner, H., Wilhelms-Dick, D., Brey, T., Abele, D., 2012. Coexistence of three calcium carbonate polymorphs in the shell of the Antarctic clam *Laternula elliptica*. Geochem. Geophys. 13, Q05014.
Newton, D.E., 2007. Chemistry of Space. Facts on File. Infobase Publishing Ltd., New York.
Parakhonskiy, B.V., Haase, A., Antolini, R., 2012. Sub-micrometer vaterite containers Synthesis, substance loading, and release. Angew. Chemie Int. Ed. 51, 1195–1197.
Perrin, A., 1970. Diversite des formes d'accumulation de la phytoferritine dans les cellules constituant l'epitheme des hydathodes de *Taraxacum officinale* Weber et *Saxifraga aizoon*. Planta 93, 71–81.
Pyankov, V.I., Kondratchuk, A.V., Shipley, B., 1999. Leaf structure and specific leaf mass: the alpine desert plants of the Eastern Pamirs, Tadjikistan. New Phytol. 143, 131–142.
Schulz, H., Baranska, M., 2007. Identification and quantification of valuable plant substances by IR and Raman spectroscopy. Vib. Spectrosc. 43, 13–25.
Smith, M., Fitch, J., 1909. *Saxifraga scardica* drawing. Curtis's Bot. Mag. 135, 8243.
Strid, A., Tan, K., 1986. Mountain Flora of Greece. Cambridge University Press.
Tkach, N., Röser, M., Miehe, G., Muellner-Riehl, A.N., Ebersbach, J., Favre, A., Hoffmann, M.H., 2015. Molecular phylogenetics, morphology and a revised classification of the complex genus *Saxifraga* (Saxifragaceae). Taxon 64, 1159–1187.
Vogelman, T.C., Nishio, J.N., Smith, W.K., 1996a. Leaves and light capture: light propagation and gradients of carbon fixation within leaves. Trends Plant Sci. 1, 65–70.
Vogelmann, T.C., Bornman, J.F., Yates, D.J., 1996b. Focusing of light by leaf epidermal cells. Physiol. Plant. 98, 43–56.
Webb, D.A., Gornall, R.J., 1989. Saxifrages of Europe. Christopher Helm, London.
Wightman, R., Wallis, S., Aston, P., 2017. Hydathode pit development in the alpine plant Saxifraga cochlearis. Flora 233, 99–108.
Zhang, Z., Xia, N., Gornall, R.J., 2015. Leaf venation patterns in the genus *Saxifraga* (Saxifragaceae). Phytotaxa 221, 123–136.